Materials & Design 215 (2022) 110446

Contents lists available at ScienceDirect

Materials & Design

journal homepage: www.elsevier.com/locate/matdes

Flexible planar metamaterials with tunable Poisson's ratios

Nicholas Pagliocca [a,1], Kazi Zahir Uddin [a,1], Ibnaj Anamika Anni [a], Chen Shen [a], George Youssef [b], Behrad Koohbor [a,c,*]

[a] Department of Mechanical Engineering, Rowan University, 201 Mullica Hill Rd., Glassboro, NJ 08028, USA
[b] Experimental Mechanics Laboratory, Department of Mechanical Engineering, San Diego State University, 5500 Campanile Drive, San Diego, CA 92182, USA
[c] Advanced Materials & Manufacturing Institute, Rowan University, Glassboro, NJ 08028, USA

HIGHLIGHTS

- Flexible planar mechanical metamaterials with tailorable properties are 3D printed.
- Mechanical behavior of structures is tuned by the introduction of orthogonal perforations.
- Correlations between unit cell geometry and the auxetic response are highlighted.
- Self-strengthening behavior of flexible structures is studied by multiscale measurements.
- Graded structures with controllable Poisson's ratios are designed and fabricated.

GRAPHICAL ABSTRACT

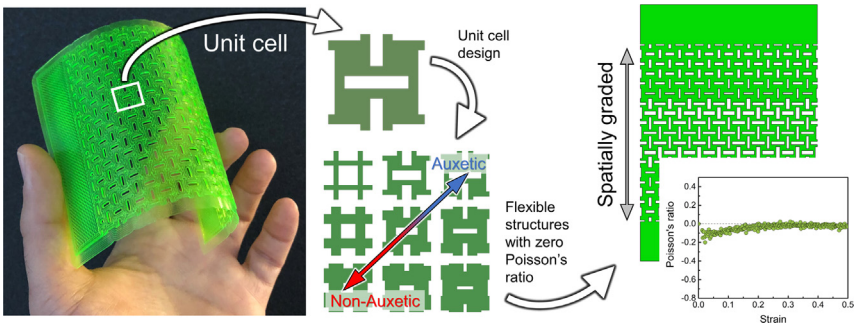

ARTICLE INFO

Article history:
Received 2 November 2021
Revised 20 January 2022
Accepted 30 January 2022
Available online 2 February 2022

Keywords:
Auxetic
Mechanical metamaterials
Multiscale characterization
Digital image correlation
Poisson's ratio

ABSTRACT

This research reports on the design, fabrication, and multiscale mechanical characterization of flexible, planar mechanical metamaterials with tailorable mechanical properties. The tunable mechanical behavior of the structures is realized through the introduction of orthogonal perforations with different geometric features. Various configurations of the perforations lead to a wide range of Poisson's ratios (from −0.8 to 0.4), load-bearing properties, and energy absorption capacities. The correlations between the configuration of the perforations and the auxetic response of the structures are highlighted through computational and experimental characterizations performed at multiple length scales. It is demonstrated that the local in-plane rotation of the solid ligaments in a uniaxially loaded structure is the primary factor that contributes to its strain-dependent auxetic behavior at macroscopic scales. Confinement of these local rotations is then used as a practical strategy to activate a self-strengthening mechanism in the auxetic structures. It is further shown that the fabrication of planar flexible structures with controllable Poisson's ratios is feasible through spatial adjustment of perforations in the structure. Finally, discussions are provided regarding the practical applications of these structures for a new generation of highly energy-absorbing protective equipment.

1. Introduction

In recent years, a significant amount of research has been dedicated to studying mechanical metamaterials to explore their properties and further exploit their functionalities in a variety of

* Corresponding author at: Department of Mechanical Engineering, Rowan University, 201 Mullica Hill Rd., Glassboro, NJ 08028, USA.
E-mail address: koohbor@rowan.edu (B. Koohbor).
[1] Authors with equal contribution.

https://doi.org/10.1016/j.matdes.2022.110446
0264-1275/

applications [1,2]. The term 'metamaterials' is broadly used to define artificial materials and structures that exhibit novel properties obtained by the combination of their constituent materials and/or their structural morphology [3]. The properties of metamaterials, as their name implies, are beyond those that are common in conventional engineering materials [4–8]. The small-scale and tunable topology of mechanical metamaterials, which exhibit high flexibility, can be leveraged to tailor their macroscale mechanical response [9]. Therefore, mechanical metamaterials reveal a route towards enhanced macroscopic properties, including higher indentation resistance, enhanced vibration damping under static and dynamic conditions, resistance to shear, high hardness, and improved fracture toughness [10–13]. Advances in mechanical metamaterials seek to understand their unique properties and explore various approaches for designing, fabricating, and optimizing the material attributes via methods that were not previously possible in conventional engineering materials [14].

Most monolithic, engineering materials experience lateral expansion (*i.e.*, positive strains) when subjected to uniaxial compression. This phenomenon is referred to as the Poisson effect and results from the intrinsic material behavior that prevents the distortion of a material under mechanical loads without altering its volume (at least during large inelastic deformations). For most conventional engineering materials, the Poisson's ratio is a positive value. However, this ratio is not required to remain positive for all material systems and in all loading conditions. According to the classical theory of elasticity for isotropic 3D structures, the Poisson's ratio can range between −1.0 to +0.5, or even higher for orthotropic and anisotropic materials [15,16]. For 2D structures, this range can be further expanded to include Poisson's ratios from −1 to +1 [17]. Materials that possess a negative Poisson's ratio (NPR) are collectively referred to as auxetics [18–20]. Mechanical and thermodynamic models predicted such behaviors as early as the 1980′s which initially led to investigations into foams with NPRs by Lakes [20–23]. Auxetic behavior has been reported in several naturally existing materials, including cancellous bone, tendons, and minerals [24–31]. In addition, similar mechanical properties have been investigated in composite structures [32] and materials with a negative coefficient of thermal expansion [33]. Due to their enhanced mechanical properties [10–13], synthetic auxetic materials have been developed and have found many potential applications, *e.g.*, in the design of biomaterials, prostheses, novel fasteners, tunable optics, next-generation actuators and sensors, and shape-memory foams with superior acoustic and damping properties [34–36]. Likewise, tunable materials with variable responses to changing environments or loading scenarios, including those with auxetic behaviors, have been investigated for many applications [37–39].The distinctive properties of auxetic materials have made them the topic of considerable research interest in soft-bodied materials and devices [40,41]. Examples include biomimetic flexible manipulators and soft-bodied cylinders fabricated from auxetic cells for angular actuation [42,43], both of which demonstrate an underlying significance of NPR.

The Poisson's ratio of auxetic mechanical metamaterials is controlled by microstructural and architectural features [11,18] rather than their composition [14]. Hence, auxetic materials can be classified based on their deformation mechanisms, where common classes include re-entrant structures, chiral structures, hierarchical laminates, polymeric foams, and rotating rigid structures [44–47]. While these structures are promising in many aspects, the availability of auxetic materials is still limited because of the costly and challenging manufacturing processes required for large-scale production. Most often, the design and development of an auxetic material require embedding a structure with a complicated geometry in a host matrix. This process is challenging to control at the microscale, leading to fabrication uncertainty or even premature material failure. Consequently, manufacturing processes have hindered the advancement of auxetic materials in industrial applications [48]. Nonetheless, the advantage of additive manufacturing provides meaningful insight into the design perspective of these scientifically exciting metamaterials. In all, the novel advanced fabrication techniques have provided an unprecedented opportunity to develop programmable metamaterials, some of which were designed recently through advanced machine learning algorithms [49–51].

Recent findings have revealed that mechanical instability in 2D planar porous structures stimulates significant geometry changes upon applying far-field loads [52,53]. For example, if a square array of circular holes in a 2D elastomeric matrix is subjected to in-plane tensile loads, the circular holes transform into mutually orthogonal ellipses [48]. The ellipses, in this case, invert periodically, allowing the structure to bend inward and display an auxetic behavior [48]. This elastic instability is repeatable over a range of applied loads. The load-induced circular-elliptical transformation discussed promotes the necessity of developing a new class of auxetic metamaterials using perforations. The introduction of perforations in regular structures to develop unique properties has been a topic of research interest since 1960 [54,55] and has become a potential system to produce structures with auxetic characteristics. In several studies, researchers have proposed several perforation patterns to achieve auxetic characteristics. For example, Grima *et al.* [15] and Bertoldi *et al.* [48] developed auxetic metamaterials using diamond and circular perforations in 2D structures. The perforated systems mimic the metamaterial behavior of rotating unit cells, including re-entrant mechanisms, chiral honeycombs, rotating squares, triangles, rectangles, and mixed shape unit cells [56–59]. Rotating square and perforated sheet structures that were proposed in [60] have also attracted significant attention and have been explored in several research papers [15,17,61–63]. Another method of introducing perforations using slits/cuts was showcased recently because of its ability to convert non-auxetic planar materials to auxetic ones [64,65]. The concept of cuts and perforations is an appealing way to generate auxetic structures with spatially tailorable properties, paving the way for low-cost auxetic material manufacturing at large scales and lowering material waste [59,66–68]. Lastly, center symmetric perforated systems have an added advantage in tuning the hierarchical configurations for tailoring mechanical properties. Previous studies have found that randomness in slit orientation also provides global auxetic behavior, a concept that has led to developing planar auxetic structures with a graded topology [69].

In addition to auxetic characteristics in mechanical metamaterials, functional gradation has been separately investigated to achieve enhanced properties with multifunctionality [70–73]. For example, honeycombs with a thickness gradient constructed from polymeric materials have been exploited experimentally and numerically in composite structures for their improved mechanical and acoustic properties [74–79]. In addition to improved energy absorption characteristics achieved by cell density gradation, inversion of cell hinges leads to an auxetic behavior, which can further enhance the mechanical response of the structure [69]. On the one hand, the symbiotic elastic deformations of the density-graded regions give rise to increased energy absorption efficiency compared to their mono-density counterparts [72,73]. The ability to develop and optimize the response of a density-graded structure for a specific application offers unique design opportunities for various use-cases such as medical orthopedic shoes or footwear in general [72]. On the other hand, the auxetic behavior is conducive for elastic instabilities with potentially significant energy absorption mechanisms, furthering improving the impact mitigation capabilities of tailored metamaterials and structures.

The present paper aims to provide an insight into the concept of strain-dependent auxetic response based on patterned perforations in a planar geometry. Perforations are tuned in the design phase to understand the hierarchical configurations of the considered geometries and how these hierarchies are reflected in the multiscale deformation response of the structures. The possibility of simultaneously tailoring the Poisson effect, load-bearing, and energy absorption performance of the structures by changing the geometrical attributes is demonstrated. It is also shown that the spatial adjustment of the perforations in the structure facilitates the design of structures with highly controllable Poisson effects. The latter concepts highlight the significance of the recently developed density gradation methodology as a promising and practical approach for tailoring the local and global mechanical properties in flexible structures.

2. Methodology

2.1. Unit cell design

Planar samples with repeating unit cells were designed and additively manufactured (*i.e.*, 3D printed). The investigated unit cells encompassed spatially arranged geometrical features of squares with different rectangular perforations. The geometric features of the unit cells are shown in Fig. 1**a**. Variation of the geometric features of the perforations leads to various mechanical properties at macroscales. The two nondimensional factors that are considered to define the basic geometry of the unit cells in this work are the aspect ratio (*AR*) and inter-cell spacing (*IS*), expressed as

$$AR = a/b \tag{1}$$

$$IS = s/L \tag{2}$$

where, *a*, *b*, *s*, and *L* denote dimensional details of a perforated unit cell, as defined in Fig. 1**a**. By varying the geometric factors *AR* and *IS*, nine different unit cell configurations were designed, as illustrated in Fig. 1**b**. The relative density of each unit cell was calculated as the ratio between the apparent density of the structure and the base material density. The base material used in this work was thermoplastic polyurethane (TPU), whose density is 1160 kg/m^3. Table 1 shows the relative densities determined for the structures. As will be discussed in the forthcoming sections, the wide range of mechanical behaviors observed in the structures is attributed to the geometric characteristics of the unit cells.

2.2. Sample fabrication and testing

Squared planar structures containing a 9 × 9 array of unit cells were 3D printed from TPU with 0.97 ± 0.04 mm thickness using a material extrusion additive manufacturing process. The base material used in this study, *i.e.*, TPU, is a hyperelastic polymer; thus the fabricated planar structures inherited similar hyperelastic behaviors, as shown in Fig. 2**a**. The mechanical properties of the base TPU polymer under tensile and compressive forces were separately characterized in-house, with details reported in **Supplementary Information**. Two 20 mm solid gripping tabs were concurrently printed at sample ends to facilitate gripping and tensile load transfer. The fabricated samples were fixed inside an electromechanical test frame (Shimadzu AGS-X with 10 kN load-cell capacity) with the aid of four tapered aluminum fixtures, attached to the samples using three bolts at each side (Fig. 2**b**). The tensile load was applied monotonically at a constant rate of 10 mm/min until failure. Sample deformation was monitored and quantified at macro and meso scales, with the aid of a dual camera digital image correlation (DIC) system. As shown in Fig. 2**c**, the two camera units were able to capture images at macro (the entire sample, Fig. 2**d**) and mesoscales (a roughly 3 × 3 array of cells located near the center of the structure, Fig. 2**e**). Time lapse images were captured from macroscale and mesoscale regions of interest at a rate of 1 frame/sec and were synchronized with the load data collection rate. Deformation fields at the two scales were analyzed using the image correlation software Vic-2D (Correlated Solutions, Inc., SC, USA) with different subset and step sizes relative to each scale.

For macroscale characterizations, the global deformation was analyzed using the perforations as the speckle pattern. A more detailed study of the deformation and strain fields developed within the solid ligaments was made possible by analyzing the images captured by the mesoscale camera. A high contrast fine speckle pattern spray painted on the sample surface prior to testing was used for this purpose (Fig. 2**e**). To avoid delamination of the speckle pattern from the surface of the highly flexible struc-

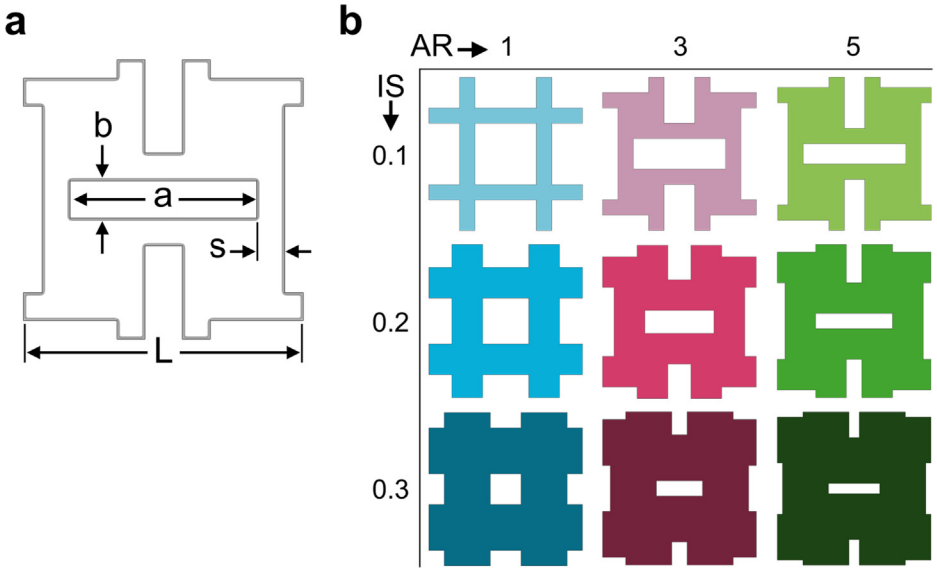

Fig. 1. (a) Geometric features of a generic unit cell with rectangular perforations. (b) The unit cells used in this study designed with various aspect ratio (*AR*) and inter-cell spacing (*IS*) values. All unit cells are square in shape and have an edge size of *L* = 10 mm.

Table 1
Relative densities determined for the unit cell designs in this work.

		Perforation Aspect Ratio (*AR*)		
		1	**3**	**5**
Inter-cell Spacing (*IS*)	**0.1**	0.36	0.52	0.64
	0.2	0.64	0.73	0.80
	0.3	0.84	0.88	0.91

tures, mechanical tests were carried out immediately after the speckle pattern application to take advantage of the ductility of the undried white paint.

The evolution of the Poisson's ratio for each structure was determined using the DIC results obtained at the macroscale. To this goal, axial (e_l) and transverse (e_t) strains developed on the surface were determined by averaging the entire collection of local strain data for every single image and for each strain component. The incremental definition of Poisson's ratio (*i.e.*, υ=-de_t/de_l) was then used to determine the evolution of Poisson's ratio during tensile loading [80,81]. The incremental (also referred to as 'tangent') definition of Poisson's ratio was used over the total (also called 'secant') definition as it provides a more realistic measure for the Poisson effect in nonlinear hyperelastic materials subjected to large deformations. Specifically, it has been reported that the secant formulation (*i.e.*, the simple ratio between - e_t and e_l) tends to underestimate the Poisson's values in nonlinear auxetic structures, including open-cell foams [81]. The exact same approach, *i.e.*, the spatial averaging of all local (nodal) strain values, was used to determine the Poisson's ratio in FE analyses.

2.3. Hybrid Computational-Experimental approach

A full scope of the deformation behavior of the structures in this work requires characterization in confined and unconfined conditions. The unconfined conditions are referred to conditions where a uniaxial load is applied, and the structure is freely deformed in the transverse directions. This condition is similar to experimental test protocols detailed in **Section 2.2**. In such cases, multiscale experimental tests are sufficient for a complete understanding of the load-bearing and auxetic characteristics of the structures. However, since the flexible structures studied in this work can be used as interlayers in multi-layered structures with tunable mechanical properties (see **Supplementary Information**), their

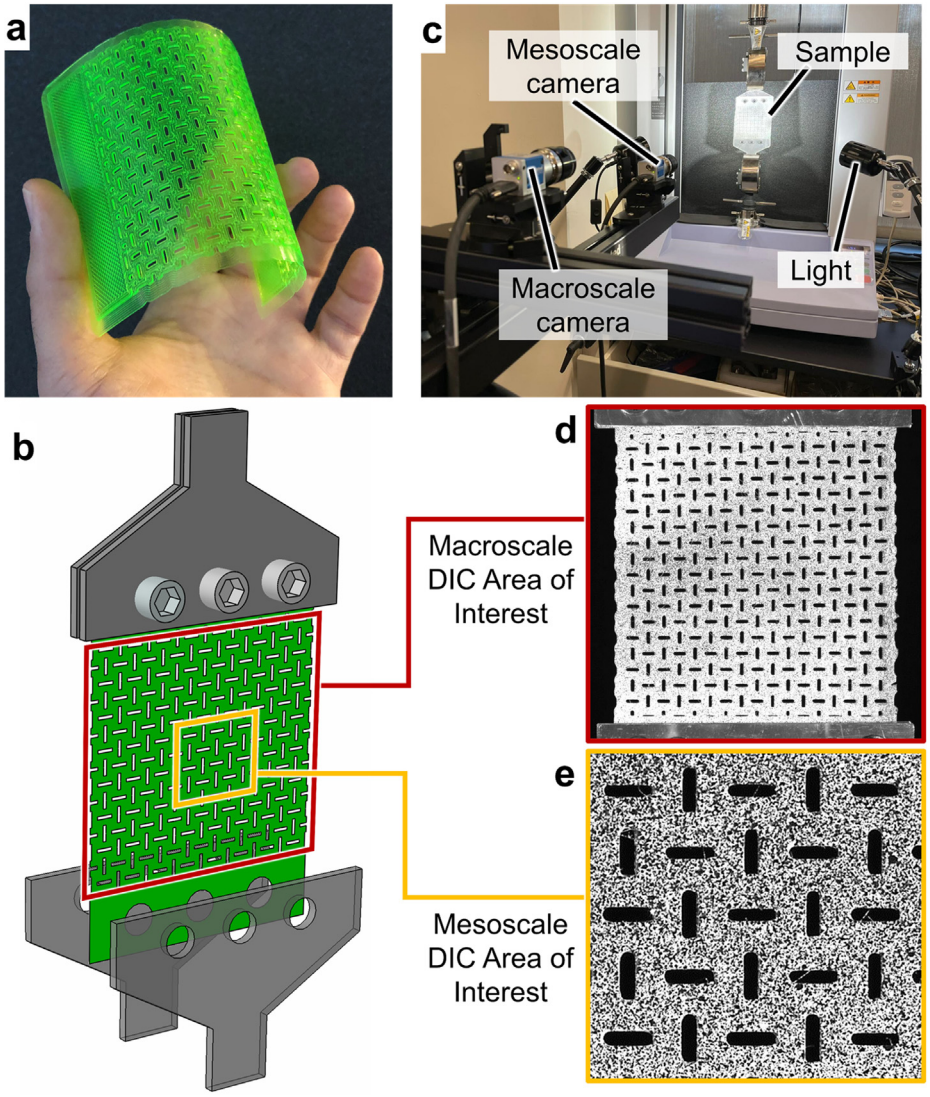

Fig. 2. (a) An example of the perforated structures after 3D printing, showing their highly flexible nature. (b) Schematic of the tapered aluminum tabs used to facilitate gripping by test frame fixtures. (c) Experimental setup showing the cameras and the areas of interest for (d) macroscale and (e) mesoscale DIC characterizations.

mechanical characteristics under *confined* conditions must also be studied. Besides, when subjected to confined loading conditions, the auxetic nature of the structures can be leveraged to promote a self-strengthening behavior that improves both load-bearing and energy dissipation characteristics of the structures [82–84].

Here, the confined conditions refer to the uniaxial loading of the structure while the lateral edges are fixed in transverse (horizontal) directions. Experimental evaluation of the structures in such conditions requires specialized test fixtures that are unavailable to the authors. Therefore, finite element (FE) analyses were used as the virtual experimental substitute to complement the experimental measurements and provide a detailed insight into the mechanics of the structures in confined conditions. Finite element analyses were performed in the commercial FE package Abaqus® using in-house measured TPU properties as input. Details of the FE model creation, element discretization, and the characterization of the base polymer are provided as **Supplementary Information**. The percentage improvement in mechanical strength (%ΔS) of the structures due to lateral confinement was quantified by the relative increase in the strength with respect to unconfined conditions, *i.e.*,

$$\%\Delta S = \frac{S^{cnf}(e_l) - S^{uncnf}(e_l)}{S^{uncnf}(e_l)} \times 100 \tag{3}$$

Where, S and e_l denote global stress and axial strain, respectively. The superscripts '*cnf*' and '*uncnf*' refer to confined and unconfined conditions, respectively. Global stress is determined as the tensile load normalized by the effective cross-sectional area of the structure. Definition of the effective cross-sectional area is provided as **Supplementary Information**. The practical application of **Eq. (3)** is to quantify the degree of strength improvement (esp. in the case of auxetic structures) in response to loading conditions applied in the presence of lateral confinements, as discussed further in **Section 3.4**.

Finally, the ideality parameter, I, was used as the metric for the energy absorption performance of the structures. As expressed in **Eq. (4)**, This parameter is often used as a metric for quantifying the ratio of the energy absorbed by the structure (*i.e.*, the stored strain energy) to the energy imposed on it (*i.e.*, the work per volume done by the applied force) [72].

$$I(e_l) = \frac{\int_0^e S(e_l)\, de}{S \times e_l} \tag{4}$$

3. Results and discussion

3.1. Multiscale measurement of deformation response

The macroscale deformation responses of two representative structures are shown in Fig. 3**a**. The structure, shown in the left column (AR = 1, IS = 0.3), indicates a conventional Poisson effect, as revealed qualitatively by the constant decrease of its width during axial loading. The other structure, shown in Fig. 3**a** (AR = 3, IS = 0.1), exemplifies a different Poisson effect, *i.e.*, auxetic or negative Poisson's ratio, since it shows lateral expansion in response to axial elongation. The macroscopic Poisson's ratios of the two representative structures were determined and are shown in Fig. 3**b**. The Poisson's ratios of the two representative structures show completely different trends at low macroscopic (global) strains. The structure with AR = 1, IS = 0.3 shows a positive Poisson's ratio with an initial value of *ca.* 0.4, decreasing to less than 0.2 at larger macroscopic strains. On the other hand, the Poisson's ratio of the structure with AR = 3, IS = 0.1 shows strong negative values (*i.e.*, an auxetic effect) at low macroscopic strains. The auxetic effect vanishes at macroscopic strains around 0.15, and the structure continues to deform in a non-auxetic manner. Some of the structures in this work exhibit an auxetic response, promoting a self-strengthening mechanism especially when deformed under confined conditions. The latter can be leveraged in designing planar structures with tunable mechanical properties, as discussed in the forthcoming sections.

The auxetic vs. non-auxetic responses can be correlated with the mesoscale deformation behavior of the structures. An example of such mesoscale deformation behaviors is shown in Fig. 3**c**, wherein the deformation fields developed over single-unit cells are measured by the mesoscale DIC system. For the non-auxetic case (AR = 1, IS = 0.3), a more uniform distribution of local axial strain, ε_{yy}, is observed. The strain uniformity is evident as the vertical cell walls undergo uniform axial deformation with no discernible bending or rotation. In contrast, the structure with rectangular perforations (*i.e.*, AR = 3) indicates a significantly more heterogeneous strain distribution, revealed in the form of (1) highly stretched unit cell ligaments and (2) rotation of the solid portions of the unit cell. The latter observation is quantified by extracting the values of local normal and shear strains and the degree of rotation developed on the solid parts of the auxetic structure. Fig. 4 shows the evolution of local axial strain, ε_{yy}, local shear strain, ε_{xy}, and the rotation angle, ω, measured in the auxetic structure with AR = 3, IS = 0.1. A $\sim 7°$ in-plane rotation measured over the solid part of the structure is identified as the main source of the auxetic behavior in the structure at global strains less than 0.15. Interestingly, the evolution of the angle of rotation is seen to approach saturation at larger global strains. This saturation is shown by a constant decrease of slope in the ω curve. A noteworthy observation in Fig. 4 is that the local strains developed on solid parts of the auxetic structure tend to dominate the rotation at larger global elongations. An inflection point is found in the local shear strain at 0.15 global strain. Interestingly, this global strain is where the auxetic structures change into a non-auxetic one (see Fig. 3**b**). The presence of such an inflection point signifies the role of local shear strains as a major mechanism controlling the auxetic behavior of the structures and remains an interesting topic of study for future research. Nevertheless, the observations made in this work are consistent with previous studies [63,66], highlighting the weakening of the auxetic behavior of the structure at global strains greater than 0.1.

3.2. FE analysis verification

FE analyses were performed to complement the multiscale experimental measurements while at the same time providing an opportunity to examine the self-strengthening behavior of the auxetic structures subjected to confined loading conditions. As the first step in achieving these goals, the FE results were verified by the multiscale experimental measurements discussed in **Section 3.1**. FE modeling results were verified by comparing the macro/mesoscale deformation patterns, global stress–strain, and Poisson's ratio evolution in the examined structures. For brevity, only the latter two comparisons are shown in the main article. Details regarding the multiscale deformation behaviors are provided as **Supplementary Information**.

A comparison between the global stress–strain responses of two representative structures is shown in Fig. 5. While model predicted curves are in acceptable agreement with experimental measurements, the slight discrepancy between the two data sets can be traced back to two main sources. First, the FE results are based on constitutive data identified by a least-square fitting of a 5th order Ogden hyperelastic model to 3D printed TPU samples tested in tension and compression. The stability of the fitted curve is bound within the maximum tensile and compressive strains applied on 3D printed TPU samples tested in-house (see **Sec. S2** in **Supplementary Information**). Therefore, local strains that

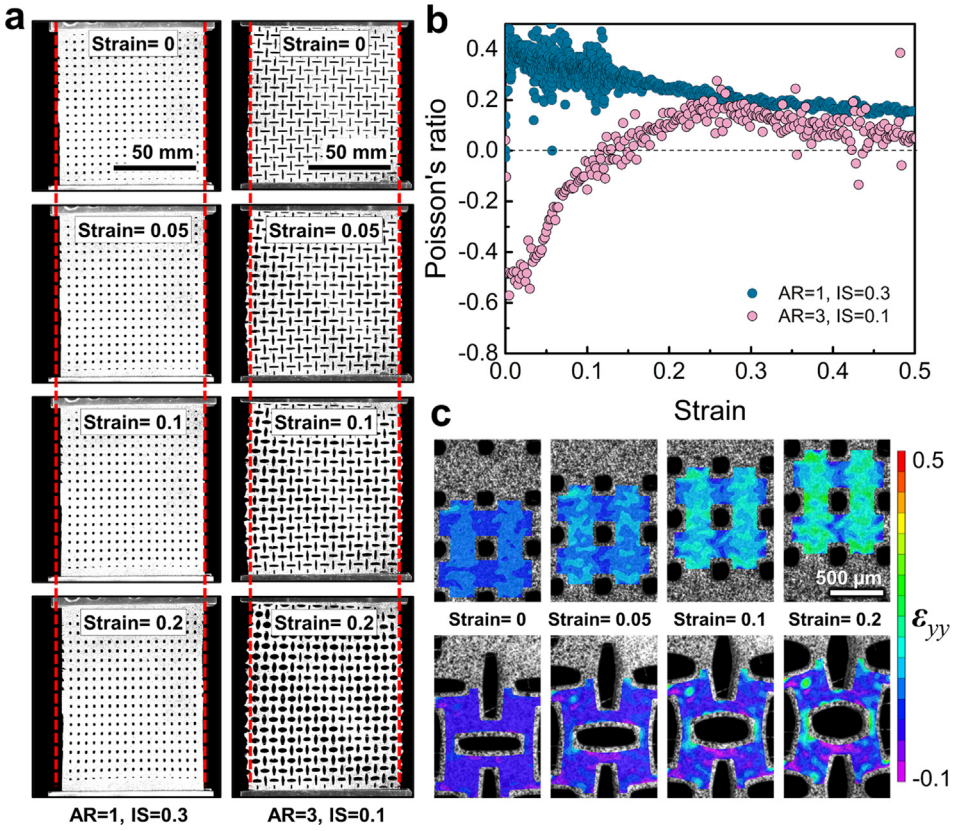

Fig. 3. (a) macroscale deformation behavior of two representative structures with *AR* = 1, *IS* = 0.3 (left) and *AR* = 3, *IS* = 0.1 (right). The vertical dashed lines mark the original width of the samples, thus, qualitatively showing the Poisson behavior. (b) Evolution of macroscopic Poisson's ratios for the two structures plotted with respect to global tensile strain applied to the structure. (c) Evolution of local axial strain, ε_{yy}, in the two examined structures, revealed by mesoscale DIC measurements.

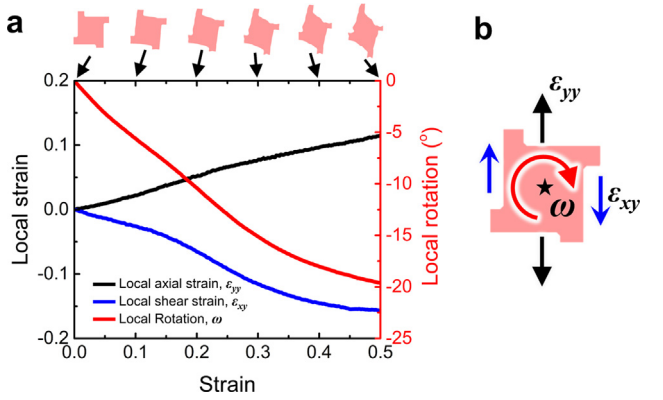

Fig. 4. (a) Evolution of local axial strain, ε_{yy}, local shear strain, ε_{xy}, and the angle of rotation, ω, as functions of the global strain applied to the structure. These parameters are measured in the auxetic structure with *AR* = 3, *IS* = 0.1. (Typical deformation patterns of the unit cell at different strains are shown at the top). The three parameters of interest are visually shown in (b). The angle of rotation has been evaluated in reference to the centroid of the element marked by the star symbol in (b).

exceed those used for curve fitting will introduce error to model predictions. Secondly, various printing defects developed during the fused filament fabrication (FFF) of the structures also contribute to the discrepancies observed between the experimental and model-predicted data in Fig. 5. Several of such printing defects were identified in this work and are discussed in **Supplementary Information**.

3.3. Poisson effect and auxetic response

The model predicted variations of Poisson's ratio as a function of strain for all examined structures are shown in Fig. 6. The dataset in this figure includes Poisson's ratios of the two structures whose experimentally measured values were shown earlier in Fig. 3**b**. As shown in Fig. 6, the model-predicted trends and values obtained for the previously examined structures resemble the experimental data, confirming the consistency between the modeling and experimental characterizations. Furthermore, the noise-free, smoother data obtained from FE models makes it possible to effectively examine the auxetic vs. non-auxetic behaviors . As such, the structures with *AR* = 3,5 and *IS* = 0.1 are identified to have strong auxetic behavior. The strong auxetic behavior of these structures is exemplified by high negative Poisson's values that remain valid over an extended strain range. The two other structures that show a relatively weak auxetic response include those with *AR* = 3,5 and *IS* = 0.2. On the other hand, strong non-auxetic behaviors are determined for structures with *AR* = 1,3 and *IS* = 0.3. Interestingly, despite the presence of many perforations in the latter two structures, which leads to a ~ 40% reduction in density (see Table 1), their stress–strain and Poisson's ratio evolutions are comparable with those of the base TPU (**Figure S3**).

3.4. Strength and energy absorption responses with and without confinement

Global stress–strain responses of the structures in unconfined conditions were determined experimentally and via FE modeling. To investigate the self-strengthening response of the structures, their stress–strain behaviors when lateral confinements are pre-

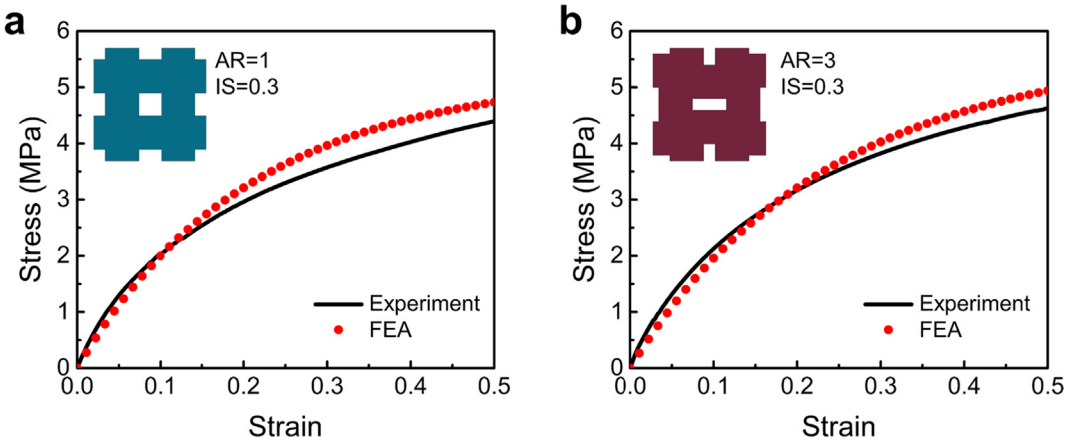

Fig. 5. A comparison between the global stress–strain responses of two representative structures with (a) *AR* = 1, *IS* = 0.3 and (b) *AR* = 3, *IS* = 0.3.

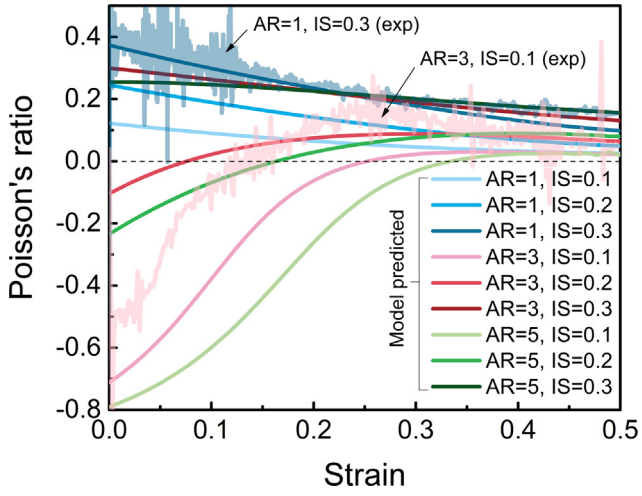

Fig. 6. Variation of Poisson's ratio with (global) strain obtained by FE simulations. Experimental curves (denoted by 'exp') for two representative structures with *AR* = 1, *IS* = 0.3 and *AR* = 3, *IS* = 0.3 are included to facilitate the comparison between the model predictions and experimental measurements.

sent are also examined. Investigating the effect of lateral confinement was only possible via modeling since an experimental setup that enables ideal confined measurements was unavailable to the authors. Therefore, our results and discussion will, hereafter, focus on FE simulation results only. Fig. 7 shows a comparison between the global stress–strain behaviors of the examined structures under unconfined and laterally confined conditions. In unconfined conditions (Fig. 7**a**), the stress–strain curves of the structures with strong auxetic behaviors (*e.g.*, *AR* = 3,5 and *IS* = 0.1) show a low initial stiffness, exemplified by a nonlinear concave shape spanning over strains of up to ca. 0.2. This behavior correlates with the rotation of the solid parts of the auxetic structures, which dominates the deformation mode at low stresses/strains (see Fig. 4). At global strains greater than 0.2 and upon the onset of the dominating effects of the local strains over cell rotations, the curves show an inflection point that marks the onset of a convex hardening behavior similar to that of the non-auxetic structures.

The aforementioned transition between rotation-dominant to local stretching evidenced in the macroscale stress–strain response of the auxetic structures signifies the self-strengthening mechanism in these structures [85–87]. This self-strengthening mechanism can be exploited through partial or full constraining of the cell rotations, which is practically possible through the application of lateral confinement. Practical conditions where such confined loading conditions exist include applications, wherein these planar structures are used as interlayers (*e.g.*, see **Sec. S1** in **Supplementary Information**). In such cases, the boundary conditions imposed by the adjacent layers can lead to partial or full confinement of the lateral deformation, thus, activating the self-strengthening mechanisms.

The stress–strain curves obtained for the fully-confined structures examined in this work are shown in Fig. 7**b**. The application of rigid lateral confinements leads to a significant increase in the load-bearing performance of the structures with strong auxetic behaviors, especially at low strains. On the other hand, the fully-confined condition is shown to have an insignificant effect on the stress–strain responses of the structures with less auxetic behaviors. The latter can be better highlighted by comparing the apparent stiffness of the structures. The term 'apparent stiffness' is used in this work as a metric to evaluate the slope of the initial portion of the stress–strain curve for each structure. Given the nonlinear response of the structures examined in this work, the so-called initial deformation regime herein refers to the part of the curve between 0 and 0.004 strain. Fig. 7**c** shows the variation of the apparent stiffness values determined for unconfined and confined conditions. As discussed above, the most significant variation in the stiffness was determined for the structures with the strongest auxetic response, *i.e.*, *AR* = 3,5 and *IS* = 0.1.

The percentage improvement in the strength of the structures calculated based on **Eq. (3)** is shown in Fig. 8. As was shown earlier, confining the lateral deformation of the auxetic structures can indeed promote a strengthening mechanism. This strengthening behavior is demonstrated by the substantial improvement in the strength of the strongly auxetic structures, especially those with *AR* = 3,5 and *IS* = 0.1, at lower strains. Furthermore, the effects of the self-strengthening mechanism can be manifested in the improvement of the energy absorption capacity of the structures. Fig. 9 shows the ideality-strain curves determined for the structures in this work. In unconfined conditions, the strong auxetic response is shown to be associated with low ideality values over extended strain values. The less than 0.5 ideality in strongly auxetic structures is indicative of the inferior energy absorption capacity of the structure compared with those of Hookean materials (*e.g.*, unidirectional composites at small strain conditions). On the other hand, when utilized in applications wherein the service conditions partially or fully confine lateral deformations, all structures examined in this work outperform Hookean materials in terms of mechanical energy absorption performance. While not examined in this work, the latter can be a promising application of these

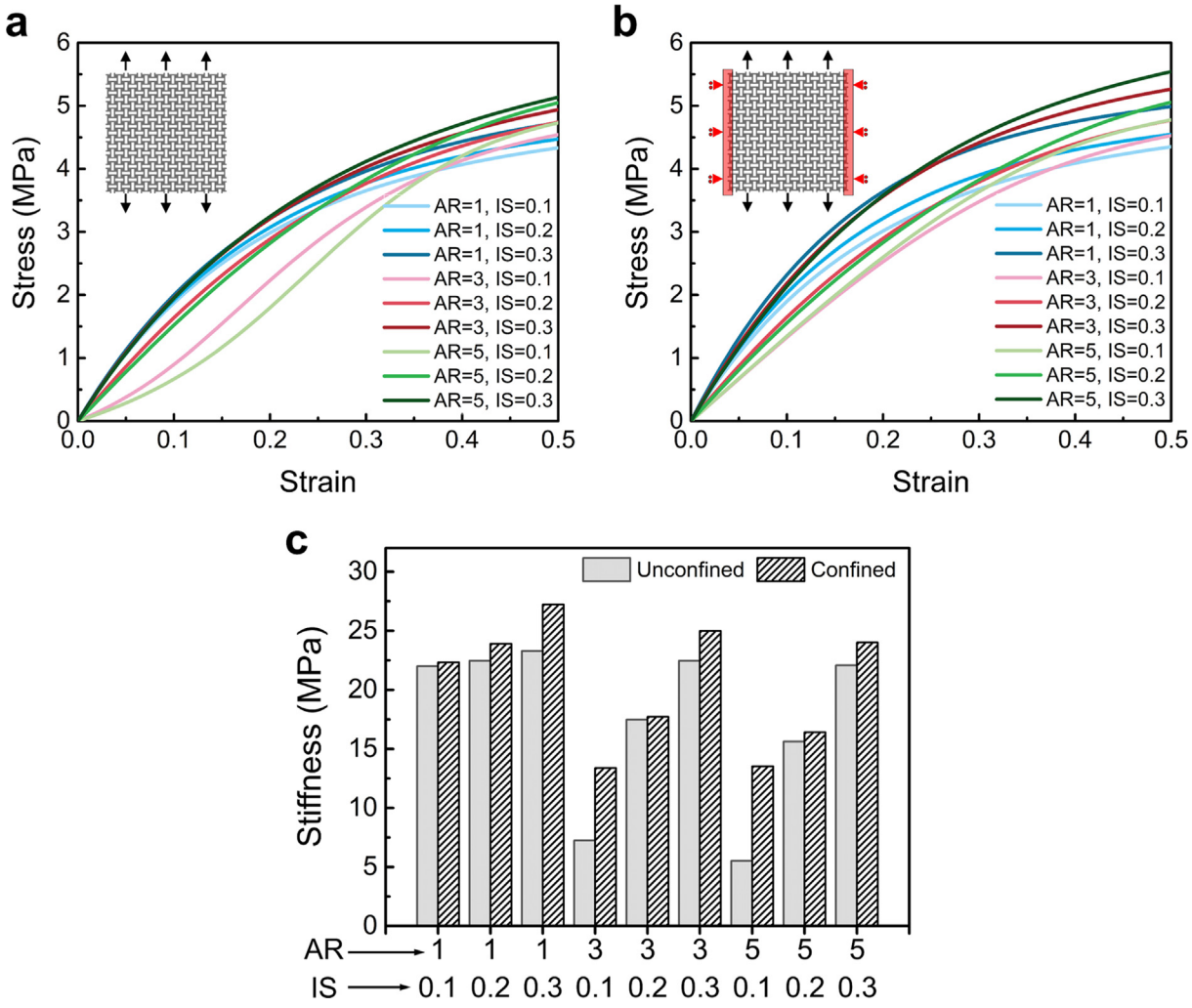

Fig. 7. Stress–strain curves obtained from FE analyses for (a) unconfined and (b) confined conditions. Graphical schemes showing the lateral constraints are shown as insets. (c) Apparent stiffness values determined for confined and unconfined loading conditions.

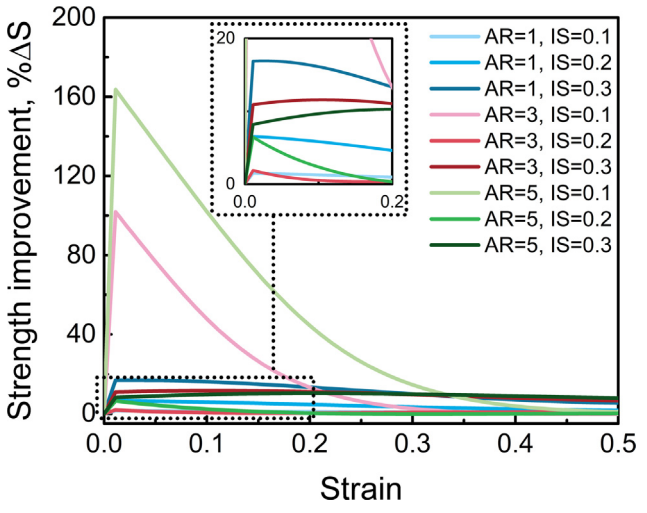

Fig. 8. Percentage improvement (with respect to unconfined conditions) in the mechanical strength of the structures due to confinement.

structures in protective applications, either as stand-alone structures or as interlayers incorporated in bulk impact mitigating components [88–90].

4. Modulating properties by spatial gradation

Various properties of the structures examined in this work were attributed to their unit cell architecture. The unit-cell dependent properties identified for these structures can be further exploited in the design of gradient structures with spatially variable tailored properties. Examples for planar mechanical metamaterials with graded perforations were recently reported by Yao *et al.* [69], wherein the spatial gradation of perforations was utilized to control the local and non-local morphology of the structures. Results obtained in the present work can also be used as input for developing planar flexible structures with spatially modulated properties. While detailed discussions on the potentials of perforation gradation are beyond the scope of this work, an example of a property tailoring approach that can be achieved by careful control of the spatial distribution of perforations is shown herein.

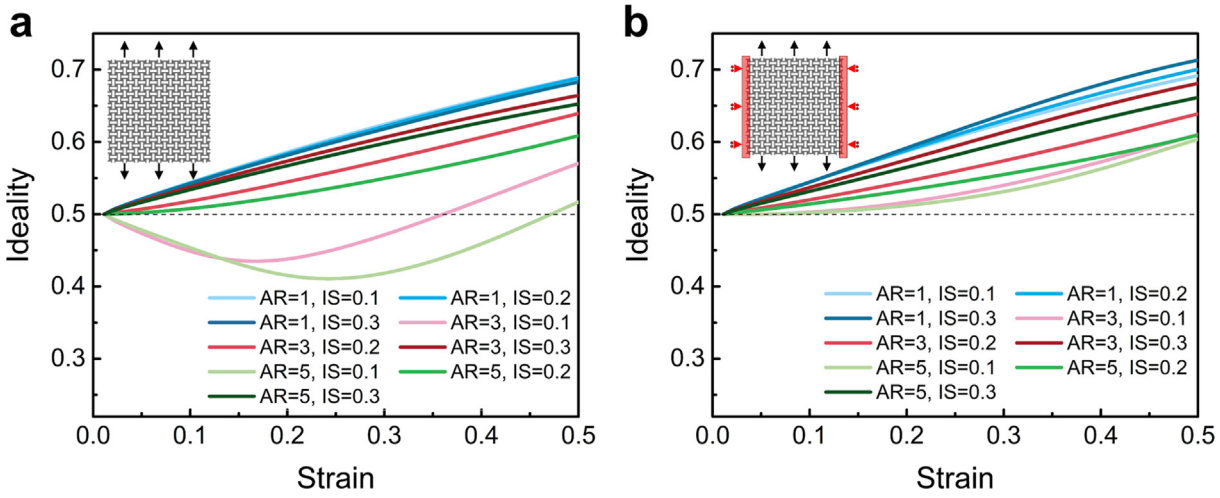

Fig. 9. Ideality-strain curves obtained for (a) unconfined and (b) confined conditions. The dashed horizontal line indicates the ideality of Hookean materials with perfectly linear stress–strain curves.

Given the Poisson's ratios shown in Fig. 6, it is possible to design structures with minimal transverse deformations. Such near-zero Poisson's ratio structures have found applications in the development of soft robotic arms [91] and can be designed through spatial control of the perforations in a planar structure. It is worth noting that near-zero Poisson's ratio can also be achieved with checkered-type patterns and stripe patterns that alternate between auxetic and non-auxetic cells [91]. As shown in Fig. 6, none of the individual structures examined in this work provide a near-zero Poisson's ratio over strains ranging up to 0.5. However, arranging them in a specific fashion makes it is possible to design piece-wise graded patterns that offer near-zero Poisson's ratios over an extended strain range. The unit cells that can be used to achieve this goal are identified by examining the structures that possess Poisson's ratios nearest to zero at each strain level, as shown in Fig. 10**a**. The four unit cells identified here (*i.e.*, those with *AR* = 3, 5 and *IS* = 0.1, 0.2) can be used as the gradients of a perforation-graded structure, as shown in Fig. 10**b**. Note that the gradient design in

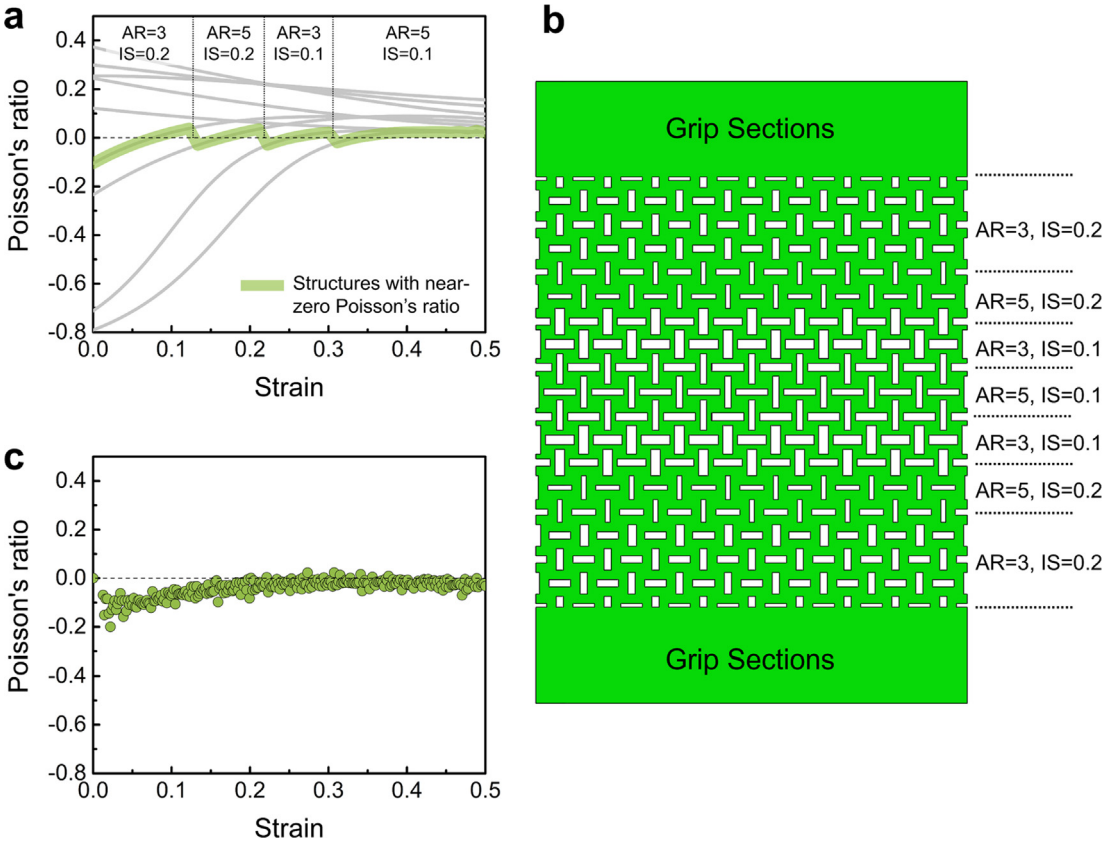

Fig. 10. (a) Identification of the unit cells that possess Poisson's ratios nearest to zero at each strain level. (b) The perforation-graded design based on the four unit cells with Poisson's ratios closest to zero. (c) Experimentally measured Poisson's ratio of the structure shown in (b), confirming a near-zero Poisson effect over an extended strain window.

Fig. 10**b** uses uniform layer widths for simplicity. Also, the layers are strategically positioned such that the adjacent layers will impose further constraints on the lateral deformation of the layers with higher auxetic responses. This is achieved by placing layers that show the highest auxetic responses at low strains towards the center of the structure and then selecting adjacent layers that approach zero at low strains in descending order from Fig. 6, as they approach the test fixtures. Between adjacent cell layers where cell perforations do not align, the dimensions of the layer closest to the center of the structure are considered to ensure uniformity between adjacent rows. The graded structure described above was fabricated and tested using the procedures described in **Section 2.2**. Fig. 10**c** shows the experimentally obtained variation of the Poisson's ratio of the perforation-graded structure over a large strain window. The results shown in this figure confirm the near-zero lateral deformations over large elongations.

The results discussed in this section are only an example that highlights the promising potentials of gradient effects in the development of tailored structures [74].While not discussed in detail, similar gradation methodologies could be used to develop materials that maintain an auxetic response over an extended strain range, or to achieve larger NPR's. Structural confinement can further enhance the response of such graded structures by offering notable strength improvements (as demonstrated and discussed in Fig. 8**)** that could be promising in many applications. It should be noted that true strength-energy absorption-density optimizations can also be achieved through similar approaches. The main challenge in such optimization processes is due to the presence of multiple variables that requires multi-objective optimizations. These studies have recently emerged as an interesting topic of research in the area of gradient optimization, especially in soft cellular materials [77,92]. Finally, the flexible and highly controllable nature of the planar structures examined in this work make them a perfect choice for use as *interface layers with tailorable properties*, a novel concept with potential applications in the design of structures with enhanced strength and impact energy mitigation characteristics. Examples of such structures can be found in the new generation of high energy-absorbing layered structures used in protective paddings, such as military helmets and sports gear and equipment [93] as well as the new generation of high-performance footwear [94]. The practical applications of the flexible structures in protective and impact mitigating structures remain an interesting topic of research to address in future studies. Nevertheless, a simple justification of the idea is proposed and is discussed in the **Supplementary Information** for the interested reader.

5. Conclusions

The mechanical behavior of flexible, planar mechanical metamaterials fabricated from thermoplastic polyurethane was examined through a multiscale experimental approach complemented with numerical modeling. Mechanical metamaterials were fabricated by 3D printing in the form of flexible sheets with various configurations of orthogonal perforations. The geometric features of the structures were shown to have a significant effect on their mechanical response. Most importantly, the Poisson behavior of the structures was shown to be strongly affected by the geometry of the perforations. The source of such behaviors was linked to deformation mechanisms at unit cell scales, revealed in this work by multiscale DIC-based analyses. In addition, the strong auxetic response of the structures was shown to lead to a self-strengthening behavior activated when the structure is deformed under lateral confinements. Finally, the potential use of structures with spatially graded perforations was revealed by designing and testing a gradient structure with near-zero Poisson ratios over an extended range of strains. While not fully explored in this work, potential applications of such flexible self-strengthening structures as interlayer materials for energy-absorbing structures were briefly discussed.

Declaration of Competing Interest

The authors declare that they have no known competing financial interests or personal relationships that could have appeared to influence the work reported in this paper.

Acknowledgements

This material is based upon work supported by the National Science Foundation under Grant No. 2035660 (B.K.) and Grant No. 2035663 (G.Y.). B.K. gratefully acknowledges the financial support provided by the Advanced Materials & Manufacturing Institute at Rowan University.

Data availability

Data will be available upon request.

Appendix A. Supplementary data

Details and discussions regarding the use of interlayers in multi-layered structures, mechanical properties of the base polymer (TPU), finite element analysis of the perforated structures and its relevant discussions on the multiscale deformation behavior of the structures, printing defects and possible sources of discrepancy between modeling and experimental measurements are provided as supplementary information. Supplementary data to this article can be found online at https://doi.org/10.1016/j.matdes.2022.110446.

References

[1] J.N. Grima, R. Caruana-Gauci, Materials that push back, Nat. Mater. 11 (7) (2012) 565–566, https://doi.org/10.1038/nmat3364.
[2] Z.G. Nicolaou, A.E. Motter, Mechanical metamaterials with negative compressibility transitions, Nat. Mater. 11 (7) (2012) 608–613, https://doi.org/10.1038/nmat3331.
[3] W. Cai, V. Shalaev, Introduction, in: W. Cai, V. Shalaev (Eds.), Optical Metamaterials, Springer New York, New York, NY, 2010, pp. 1–10, https://doi.org/10.1007/978-1-4419-1151-3_1.
[4] H.M.A. Kolken, A.A. Zadpoor, Auxetic mechanical metamaterials, RSC Adv. 7 (9) (2017) 5111–5129, https://doi.org/10.1039/C6RA27333E.
[5] A.S. Maier, World Scientific Handbook of Metamaterials and Plasmonics, Volume 2: Elastic, Acoustic, and Seismic Metamaterials, Series: World Scientific Series in Nanoscience and Nanotechnology Volume 16, World Scientific (2017), https://doi.org/10.1142/10642-vol2.
[6] F. Capolino, Theory and Phenomena of Metamaterials, Series: Metamaterials Handbook, CRC Press, 2009. http://doi.org/10.1201/9781420054262.
[7] F. Capolino, Applications of Metamaterials, Series: Metamaterials Handbook, CRC Press, 2009. http://doi.org/10.1201/9781420054248.
[8] V. Slesarenko, Planar Mechanical Metamaterials with Embedded Permanent Magnets, Materials 13 (2020) 1313, https://doi.org/10.3390/ma13061313.
[9] J.-H. Lee, J.P. Singer, E.L. Thomas, Micro-/nanostructured mechanical metamaterials, Adv. Mater. 24 (36) (2012) 4782–4810, https://doi.org/10.1002/adma.201201644.
[10] Y. Prawoto, Seeing auxetic materials from the mechanics point of view: a structural review on the negative Poisson's ratio, Comput. Mater. Sci. 58 (2012) 140–153, https://doi.org/10.1016/j.commatsci.2012.02.012.
[11] A. Alderson, A triumph of lateral thought, Chem. Ind. (London) 17 (1999) 384–391.
[12] J. Schwerdtfeger, P. Heinl, R.F. Singer, C. Körner, Auxetic cellular structures through selective electron-beam melting, Physica Status Solidi (b) 247 (2) (2010) 269–272.
[13] S. Linforth, T. Ngo, P. Tran, D. Ruan, R. Odish, Investigation of the auxetic oval structure for energy absorption through quasi-static and dynamic experiments, Int. J. Impact Eng. 147 (2021) 103741, https://doi.org/10.1016/j.ijimpeng.2020.103741.

[14] S. Babaee, J. Shim, J.C. Weaver, E.R. Chen, N. Patel, K. Bertoldi, 3D soft metamaterials with negative Poisson's ratio, Adv. Mater. 25 (36) (2013) 5044–5049, https://doi.org/10.1002/adma.201301986.
[15] J.N. Grima, R. Gatt, Perforated sheets exhibiting negative Poisson's ratios, Adv. Eng. Mater. 12 (6) (2010) 460–464, https://doi.org/10.1002/adem.201000005.
[16] T.C.T. Ting, T. Chen, Poisson's ratio for anisotropic elastic materials can have no bounds, Quart. J. Mech. Appl. Matham. 58 (2005) 73–82, https://doi.org/10.1093/qjmamj/hbh021.
[17] P.U. Kelkar, H.S. Kim, K.-H. Cho, J.Y. Kwak, C.-Y. Kang, H.-C. Song, Cellular Auxetic Structures for Mechanical Metamaterials. A Review, Sensors 20 (2020) 3132-, https://doi.org/10.3390/s20113132.
[18] K.E. Evans, M.A. Nkansah, I.J. Hutchinson, S.C. Rogers, Molecular Network Design, Nature, 353 (1991) 124–124. http://doi.org/10.1038/353124a0.
[19] X. Ren, R. Das, P. Tran, T.D. Ngo, Y.M. Xie, Auxetic metamaterials and structures: a review, Smart Mater. Struct. 27 (2) (2018) 023001, https://doi.org/10.1088/1361-665X/aaa61c.
[20] R. Lakes, Foam Structures with a Negative Poisson's Ratio, Science 235 (4792) (1987) 1038–1040.
[21] L.J. Gibson, M.F. Ashby, G.S. Schajer, C.I. Robertson, The Mechanics of Two-Dimensional Cellular Materials, Proceed. Royal Soc. Lond. Ser. A, Mathem. Phys. Sci., 382 (1982) 25–42. http://doi.org/10.1098/rspa.1982.0087.
[22] R. Almgren, An isotropic three-dimensional structure with Poisson's ratio =−1, J. Elast. 15 (1985) 427–430, https://doi.org/10.1007/BF00042531.
[23] K.W. Wojciechowski, Constant thermodynamic tension Monte Carlo studies of elastic properties of a two-dimensional system of hard cyclic hexamers, Mol. Phys., 61 (1987) 1247–1258. https://doi.org/10.1080/00268978700101761.
[24] J.L. Williams, J.L. Lewis, Properties and an anisotropic model of cancellous bone from the proximal tibial epiphysis, J. Biomech. Eng. 104 (1982) 50–56, https://doi.org/10.1115/1.3138303.
[25] R. Gatt, M. Vella Wood, A. Gatt, F. Zarb, C. Formosa, K.M. Azzopardi, A. Casha, T. P. Agius, P. Schembri-Wismayer, L. Attard, N. Chockalingam, J.N. Grima, Negative Poisson's ratios in tendons: an unexpected mechanical response, Acta Biomater. 24 (2015) 201–208, https://doi.org/10.1016/j.actbio.2015.06.018.
[26] N.R. Keskar, J.R. Chelikowsky, Negative Poisson ratios in crystalline SiO 2 from first-principles calculations, Nature 358 (6383) (1992) 222–224, https://doi.org/10.1038/358222a0.
[27] H. Kimizuka, H. Kaburaki, Y. Kogure, Mechanism for negative Poisson ratios over the α-β transition of cristobalite, SiO 2: a molecular-dynamics study, Phys. Rev. Lett. 84 (2000) 5548, https://doi.org/10.1103/PhysRevLett.84.5548.
[28] J.N. Grima, R. Gatt, V. Zammit, J.J. Williams, K.E. Evans, A. Alderson, R.I. Walton, Natrolite: A zeolite with negative Poisson's ratios, Am. Inst. Phys. 101 (8) (2007) 086102, https://doi.org/10.1063/1.2718879.
[29] R.H. Baughman, J.M. Shacklette, A.A. Zakhidov, S. Stafström, Negative Poisson's ratios as a common feature of cubic metals, Nature 392 (6674) (1998) 362–365, https://doi.org/10.1038/32842.
[30] F. Song, J. Zhou, X. Xu, Y. Xu, Y. Bai, Effect of a negative Poisson ratio in the tension of ceramics, Phys. Rev. Lett. 100 (2008), https://doi.org/10.1103/PhysRevLett.100.245502 245502.
[31] X. Tan, E. Aulbach, W. Jo, T. Granzow, J. Kling, M. Marsilius, H.-J. Kleebe, J. Rödel, Effect of uniaxial stress on ferroelectric behavior of (Bi 1/2 Na 1/2) TiO 3-based lead-free piezoelectric ceramics, J. Appl. Phys. 106 (4) (2009) 044107, https://doi.org/10.1063/1.3207827.
[32] H. Jopek, T. Strek, Thermoauxetic Behavior of Composite Structures, Materials 11 (2018) 294-, https://doi.org/10.3390/ma11020294.
[33] T.C. Lim, 2D Metamaterial with in-Plane Positive and Negative Thermal Expansion and Thermal Shearing Based on Interconnected Alternating Bimaterials, Mater. Res. Expr., 6 (2019) 115804–. http:doi.org/.
[34] J.B. Choi, R.S. Lakes, Design of a fastener based on negative Poisson's ratio foam, Cell. Polym. 10 (1991) 205–212.
[35] F. Scarpa, Auxetic materials for bioprostheses [In the Spotlight], IEEE Signal Process Mag. 25 (5) (2008) 128–1126, https://doi.org/10.1109/MSP.2008.926663.
[36] O. Sigmund, S. Torquato, I.A. Aksay, On the design of 1–3 piezocomposites using topology optimization, J. Mater. Res. 13 (4) (1998) 1038–1048, https://doi.org/10.1557/JMR.1998.0145.
[37] T.C. Lim, Auxetic Materials and Structures 1st ed, Springer Singapore, 2015. http://doi.org/10.1007/978-981-287-275-3.
[38] J.N. Grima, R. Caruana-Gauci, M.R. Dudek, K.W. Wojciechowski, R. Gatt, Smart metamaterials with tunable auxetic and other properties, Smart Mater. Struct. 22 (8) (2013) 084016, https://doi.org/10.1088/0964-1726/22/8/084016.
[39] H. Jopek, T. Strek, Thermal and structural dependence of auxetic properties of composite materials: Thermal and structural dependence of auxetic properties, Phys. Status Solidi B 252 (7) (2015) 1551–1558.
[40] J.K. Wilt, C. Yang, G.X. Gu, Accelerating auxetic metamaterial design with deep learning, Adv. Eng. Mater. 22 (5) (2020) 1901266, https://doi.org/10.1002/adem.201901266.
[41] S. Janbaz, F.S.L. Bobbert, M.J. Mirzaali, A.A. Zadpoor, Ultra-programmable buckling-driven soft cellular mechanisms, Mater. Horiz. 6 (6) (2019) 1138–1147, https://doi.org/10.1039/C9MH00125E.
[42] D. Rus, M.T. Tolley, Design, fabrication and control of soft robots, Nature 521 (7553) (2015) 467–475, https://doi.org/10.1038/nature14543.
[43] A. Lazarus, P.M. Reis, Soft actuation of structured cylinders through auxetic behavior, Adv. Eng. Mater. 17 (6) (2015) 815–820, https://doi.org/10.1002/adem.201400433.
[44] K.E. Evans, A. Alderson, Auxetic materials: functional materials and structures from lateral thinking!, Adv Mater. 12 (2000) 617–628, https://doi.org/10.1002/(SICI)1521-4095(200005)12:9<617::AID-ADMA617>3.0.CO;2-3.
[45] J.N. Grima, R. Gatt, A. Alderson, K.E. Evans, On the potential of connected stars as auxetic systems, Mol. Simul. 31 (13) (2005) 925–935, https://doi.org/10.1080/08927020500401139.
[46] X. Hou, V.V. Silberschmidt, Metamaterials with negative poisson's ratio: A review of mechanical properties and deformation mechanisms, Mech. Adv. Mater. (2015) 155–179, https://doi.org/10.1007/978-3-319-17118-0_7.
[47] G.W. Milton, Composite materials with Poisson's ratios close to—1, J. Mech. Phys. Solids 40 (5) (1992) 1105–1137, https://doi.org/10.1016/0022-5096(92)90063-8.
[48] K. Bertoldi, P.M. Reis, S. Willshaw, T. Mullin, Negative Poisson's ratio behavior induced by an elastic instability, Adv. Mater. 22 (3) (2010) 361–366, https://doi.org/10.1002/adma.200901956.
[49] R. Hedayati, A.M. Leeflang, A.A. Zadpoor, Additively manufactured metallic pentamode meta-materials, Appl. Phys. Lett. 110 (9) (2017) 091905, https://doi.org/10.1063/1.4977561.
[50] H. Li, Z. Luo, L. Gao, P.D. Walker, Engineering, Topology optimization for functionally graded cellular composites with metamaterials by level sets, Comput. Methods Appl. Mech. Eng. 328 (2018) 340–364, https://doi.org/10.1016/j.cma.2017.09.008.
[51] C. Pan, Y. Han, J. Lu, Design and optimization of lattice structures: A review, J. Appl. Sci. 10 (2020) 6374, https://doi.org/10.3390/app10186374.
[52] T. Mullin, S. Deschanel, K. Bertoldi, M.C. Boyce, Pattern transformation triggered by deformation, Phys. Rev. Lett. 99 (2007), https://doi.org/10.1103/PhysRevLett.99.084301 084301.
[53] K. Bertoldi, M.C. Boyce, S. Deschanel, S.M. Prange, T. Mullin, Mechanics of deformation-triggered pattern transformations and superelastic behavior in periodic elastomeric structures, J. Mech. Phys. Solids 56 (8) (2008) 2642–2668, https://doi.org/10.1016/j.jmps.2008.03.006.
[54] R. Bailey, R. Hicks, Behaviour of perforated plates under plane stress, J. Mech. Eng. Sci. 2 (2) (1960) 143–165, https://doi.org/10.1243/JMES_JOUR_1960_002_023_02.
[55] W.J. O'Donnell, B.F. Langer, Design of perforated plates, Journal of Engineering for Industry (US) Continues in part Trans, ASME 84 (3) (1962) 307–319, https://doi.org/10.1115/1.3667483.
[56] M. Taylor, L. Francesconi, M. Gerendás, A. Shanian, C. Carson, K. Bertoldi, Low porosity metallic periodic structures with negative Poisson's ratio, Adv. Mater. 26 (15) (2014) 2365–2370, https://doi.org/10.1002/adma.201304464.
[57] B. Florijn, C. Coulais, M. van Hecke, Programmable mechanical metamaterials, Phys. Rev. Lett. 113 (2014) 175503, https://doi.org/10.1103/PhysRevLett.113.175503.
[58] W. Ripplinger, M. Schwarz, S. Diebels, H.G. Herrmann, Auxetic aluminum sheets in lightweight structures, Mater. Testing 60 (2018) 1071–1076, https://doi.org/10.3139/120.111250.
[59] S. Shan, S.H. Kang, Z. Zhao, L. Fang, K. Bertoldi, Design of planar isotropic negative Poisson's ratio structures, Extreme Mech. Lett. 4 (2015) 96–102, https://doi.org/10.1016/j.eml.2015.05.002.
[60] J.N. Grima, K.E. Evans, Auxetic behavior from rotating squares, J. Mater. Sci. Lett. 19 (2000) 1563–1565, https://doi.org/10.1023/A:1006781224002.
[61] T.-C. Lim, Analogies across auxetic models based on deformation mechanism, Phys. Status Solidi RRL 11 (6) (2017) 1600440, https://doi.org/10.1002/pssr.201600440.
[62] J.N. Grima-Cornish, D. Attard, J.N. Grima, K.E. Evans, Auxetic Behavior and Other Negative Thermomechanical Properties from Rotating Rigid Units, Phys. Status Solidi RRL (2021) 2100322, https://doi.org/10.1002/pssr.202100322.
[63] J.N. Grima, A. Alderson, K.E. Evans, Auxetic behaviour from rotating rigid units, Physics Status Solidi (b) 242 (3) (2005) 561–575.
[64] Y. Chen, T. Li, F. Scarpa, L. Wang, Mechanically Tunable Poisson's Ratio for Vibration Control, Phys. Rev. Appl 7 (2017), https://doi.org/10.1103/PhysRevApplied.7.024012 024012.
[65] J.N. Grima-Cornish, R. Cauchi, D. Attard, R. Gatt, J.N. Grima, Smart Honeycomb "Mechanical Metamaterials" with Tunable Poisson's Ratios, Physica Status Solidi (b) 257 (10) (2020) 1900707.
[66] J.N. Grima, L. Mizzi, K.M. Azzopardi, R. Gatt, Auxetic Perforated Mechanical Metamaterials with Randomly Oriented Cuts, Adv. Mater. 28 (2) (2016) 385–389, https://doi.org/10.1002/adma.201503653.
[67] K. Billon, I. Zampetakis, F. Scarpa, M. Ouisse, E. Sadoulet-Reboul, M. Collet, A. Perriman, A. Hetherington, Mechanics and band gaps in hierarchical auxetic rectangular perforated composite metamaterials, Compos. Struct. 160 (2017) 1042–1050, https://doi.org/10.1016/j.compstruct.2016.10.121.
[68] A. Slann, W. White, F. Scarpa, K. Boba, I. Farrow, Cellular plates with auxetic rectangular perforations, Physica Status Solidi (b) 252 (7) (2015) 1533–1539.
[69] J. Yao, R. Sun, F. Scarpa, C. Remillat, Y.u. Gao, Y. Su, Two-dimensional graded metamaterials with auxetic rectangular perforations, Compos. Struct. 261 (2021) 113313, https://doi.org/10.1016/j.compstruct.2020.113313.
[70] M. Naebe, K. Shirvanimoghaddam, Functionally graded materials: A review of fabrication and properties, Applied, Mater. Today 5 (2016) 223–245, https://doi.org/10.1016/j.apmt.2016.10.001.
[71] K.Z. Uddin, B. Koohbor, Gradient optimization of transversely graded Ti-TiB structures for enhanced fracture resistance, Int. J. Mech. Sci. 187 (2020) 105917, https://doi.org/10.1016/j.ijmecsci.2020.105917.
[72] K.Z. Uddin, G. Youssef, M. Trkov, H. Seyyedhosseinzadeh, B. Koohbor, Gradient optimization of multi-layered density-graded foam laminates for footwear

material design, J. Biomech. 109 (2020) 109950, https://doi.org/10.1016/j.jbiomech.2020.109950.
[73] B. Koohbor, A. Kidane, Design optimization of continuously and discretely graded foam materials for efficient energy absorption, Mater. Des. 102 (2016) 151–161, https://doi.org/10.1016/j.matdes.2016.04.031.
[74] O. Rahman, K.Z. Uddin, J. Muthulingam, G. Youssef, C. Shen, B. Koohbor, Density-Graded Cellular Solids: Mechanics, Fabrication, and Applications, Adv. Eng. Mater. 24 (1) (2022) 2100646, https://doi.org/10.1002/adem.202100646.
[75] C. Lira, F. Scarpa, Transverse shear stiffness of thickness gradient honeycombs, Compos. Sci. Technol. 70 (6) (2010) 930–936, https://doi.org/10.1016/j.compscitech.2010.02.007.
[76] L. Boldrin, S. Hummel, F. Scarpa, D. Di Maio, C. Lira, M. Ruzzene, C.D.L. Remillat, T.C. Lim, R. Rajasekaran, S. Patsias, Dynamic behaviour of auxetic gradient composite hexagonal honeycombs, Compos. Struct. 149 (2016) 114–124, https://doi.org/10.1016/j.compstruct.2016.03.044.
[77] O. Rahman, B. Koohbor, Optimization of energy absorption performance of polymer honeycombs by density gradation, Compos. Part C: Open Access 3 (2020) 100052, https://doi.org/10.1016/j.jcomc.2020.100052.
[78] M.S. Mazloomi, M. Ranjbar, L. Boldrin, F. Scarpa, S. Patsias, N. Ozada, Vibroacoustics of 2D gradient auxetic hexagonal honeycomb sandwich panels, Compos. Struct. 187 (2018) 593–603, https://doi.org/10.1016/j.compstruct.2017.10.077.
[79] A.B.M. Supian, S.M. Sapuan, M.Y.M. Zuhri, E.S. Zainudin, H.H. Ya, Hybrid reinforced thermoset polymer composite in energy absorption tube application: A review, Defence Technol. 14 (4) (2018) 291–305, https://doi.org/10.1016/j.dt.2018.04.004.
[80] B. Koohbor, A. Blourchian, K.Z. Uddin, G. Youssef, Characterization of energy absorption and strain rate sensitivity of a novel elastomeric polyurea foam, Adv. Eng. Mater. 23 (1) (2021) 2000797, https://doi.org/10.1002/adem.202000797.
[81] S. Koumlis, L. Lamberson, Strain rate dependent compressive response of open-cell polyurethane foam, Exp. Mech. 59 (7) (2019) 1087–1103, https://doi.org/10.1007/s11340-019-00521-3.
[82] A. Papadopoulou, J. Laucks, S. Tibbits, Auxetic materials in design and architecture, Nat. Rev. Mater. 2 (2017) 1–3, https://doi.org/10.1038/natrevmats.2017.78.
[83] M. Shokri Rad, H. Hatami, R. Alipouri, A. Farokhi Nejad, F. Omidinasab, Determination of energy absorption in different cellular auxetic structures, Mech. Industry 20 (3) (2019) 302, https://doi.org/10.1051/meca/2019019.
[84] M. Sanami, N. Ravirala, K. Alderson, A. Alderson, Auxetic materials for sports applications, Procedia Eng. 72 (2014) 453–458, https://doi.org/10.1016/j.proeng.2014.06.079.
[85] Y. Jiang, Y. Li, 3D printed chiral cellular solids with amplified auxetic effects due to elevated internal rotation, Adv. Eng. Mater. 19 (2) (2017) 1600609, https://doi.org/10.1002/adem.201600609.
[86] H. Bahaloo, Y. Li, Micropolar modeling of auxetic chiral lattices with tunable internal rotation, J. Appl. Mech. 86 (2019) 041002, https://doi.org/10.1115/1.4042428.
[87] C. Körner, Y. Liebold-Ribeiro, A systematic approach to identify cellular auxetic materials, Smart Mater. Struct. 24 (2) (2015) 025013, https://doi.org/10.1088/0964-1726/24/2/025013.
[88] S. Yuan, C.K. Chua, K. Zhou, 3D-printed mechanical metamaterials with high energy absorption, Adv. Mater. Technol. 4 (3) (2019) 1800419, https://doi.org/10.1002/admt.201800419.
[89] B. Katona, A. Szlancsik, T. Tábi, I.N. Orbulov, Compressive characteristics and low frequency damping of aluminium matrix syntactic foams, Mater. Sci. Eng., A 739 (2019) 140–148, https://doi.org/10.1016/j.msea.2018.10.014.
[90] S. Cui, B. Gong, Q. Ding, Y. Sun, F. Ren, X. Liu, Q. Yan, H. Yang, X. Wang, B. Song, Mechanical metamaterials foams with tunable negative poisson's ratio for enhanced energy absorption and damage resistance, Materials 11 (2018) 1869, https://doi.org/10.3390/ma11101869.
[91] R. Hedayati, A. Güven, S. van der Zwaag, 3D gradient auxetic soft mechanical metamaterials fabricated by additive manufacturing, Appllied Physics Letters 118 (14) (2021) 141904, https://doi.org/10.1063/5.0043286.
[92] S.R. Bates, I.R. Farrow, R.S. Trask, Design, Compressive behaviour of 3D printed thermoplastic polyurethane honeycombs with graded densities, Mater. Des. 162 (2019) 130–142, https://doi.org/10.1016/j.matdes.2018.11.019.
[93] Y.K. Kim, V.B. Chalivendra, A.F. Lewis, B. Fasel, Designing flocked energy-absorbing material layers into sport and military helmet pads, Textile Res. J. (2021), https://doi.org/10.1177/00405175211010689.
[94] G.T. Burns, N. Tam, Is it the shoes? A simple proposal for regulating footwear in road running, British J. Sports Med. 54 (8) (2020) 439–440, https://doi.org/10.1136/bjsports-2018-100480.